LLNL Technical Report
UCRL-ID-116660
Filed 1994, but written May 1989

Refractive Index Change in Dissociating Shocked Benzene

David J. Erskine

Lawrence Livermore Laboratory

A calculation is made of the refractive index of a shocked solution of hydrocarbon species and spheroidal carbon particles that would be the dissociation products of benzene. The result is evaluated for benzene shocked to 15 GPa, both for an arbitrary endpoint distribution of products and reactant, and for a specific endpoint distribution suggested by a statistical-mechanical calculation. In the case of diamond particles, the refractive index is predicted to decrease by a small amount (from 1.96 to 1.75) as the dissociation proceeds. In the case of graphite particles of large oblateness, the refractive index could increase significantly through the dissociation (from 1.96 to 2.75 for infinitely oblate platelets). Thus the measurement of the time dependant refractive index through the dissociation of shocked benzene can indicate the morphology of the carbon particulates as well as the time scale for this reaction. We propose using the refractive index as a measure of completion of the dissociation reaction. This would allow a determination of the instantaneous amount of carbon in particulate form, information which is valuable in conjunction with Mie scattering experiments for example.

Introduction

Recent experiments[1] have been performed measuring the optical absorption spectra of shocked benzene. The goal of these experiments was to detect, through the scattering of light, the formation of carbon particulates predicted to occur in the decomposition of hydrocarbons under shock. Information that is presently unknown, for example, is the number density, size, growth rate and solid phase of the carbon particulates. According to the Mie theory of the scattering of light, the amount of light scattered away from the transmitted beam will depend on both the size and number density of particles. Thus, using this absorption data alone it is not possible to uniquely determine both the particle size and total amount of carbon that is in particulate form. However, by measuring the time dependant refractive index of the shocked solution, it is possible to determine the instantaneous amount of particulate carbon.

In this way, we propose using the refractive index as a measure of completion of a chemical reaction, by comparing its instantaneous value to its initial and final values. This will provide valuable information on the reaction rates of chemical reactions uniformly initiated at a well-defined time by shock. Such information will be useful in interpreting data from other optical measurements that probe the chemical dynamics behind a shock front, such as Raman or Mie Scattering experiments.

In addition, in the case of dissociating benzene and other hydrocarbons, the magnitude of the refractive index change is calculated to be strongly dependant on the morphology of the carbon particles produced. Thus, this measurement can be a valuable independent diagnostic as well. This technique is in principle applicable to any transparent reactive media.

In this paper we develop a prescription for calculating the refractive index n of the shocked fluid for an arbitrary product species distribution of shocked hydrocarbons and ellipsoidal carbon particulates using best estimates of the relevant material parameters and their pressure dependencies. In addition, we evaluate the result for a specific endpoint product distribution suggested by statistical-mechanical equilibrium calculations[2]. Our result for the initial and final indices (n_i, n_f) for 15 GPa benzene is that if the carbon particulates are diamond spherules, then $n_f<n_i$ by a small amount. However, if the particulates are graphitic platelets we find that $n_f>n_i$ by a significant amount. Thus measuring the time dependant refractive index, in addition to characterizing the time scale of dissociation and thereby providing important information on reaction rates, can indicate the morphology and material phase of the particles simply by the polarity of the effect.

An Endpoint Product Distribution

We wish to evaluate the refractive index of benzene shocked to 15 GPa since, in addition to providing a concrete example, those are the conditions that correspond to the aforementioned Mie scattering experiment[1]. Unfortunately, there is little factual data on the endpoint product distribution we could expect for benzene under those particular conditions. The most relevant information we can apply is a statistical-mechanical calculation for benzene shocked to 70.6 GPa and 4030K by Nellis[2] et al.. The calculation was made assuming a highest alkane (C_mH_{2m+2}) species of m carbon atoms, for m up to 5. The results are reproduced in Table 1. We note that by several orders of magnitude the alkanes are the dominant hydrocarbon species, compared to alkenes and alkynes. The amount of free carbon (in the form of diamond in this calculation) is approximately 4 moles per mole benzene, and insensitive to m for $m>2$.

We estimate that for benzene shocked to 15 GPa, the temperature would be in the neighborhood of 1500K. The authors[3] suggest that if their calculation were repeated for

our conditions, a similar distribution may be produced, since decreasing temperatures would favor larger alkanes, but decreasing pressures would have the opposite effect. So in addition to calculating the refractive index for an arbitrary product distribution, we will also evaluate it for the particular endpoint given by Table 1 with m=5.

Table 1. **Calculated[3] Dissociation products of benzene** (in moles) per mole of reactant benzene at 4730K and 70.6 GPa. m is the largest alkane species included in the calculation.

m	2	3	4	5
Diamond	4.07	3.87	3.86	3.84
H_2	.093	.124	.13	.142
C_6H_6	1.51e-5	8.49e-7	7.55e-7	6.51e-7
CH_4	.0247	.00779	.00754	.00728
C_2H_2	1.28e-6	6.08e-7	5.89e-7	5.60e-7
C_2H_4	8.58e-4	1.96e-4	1.86e-4	1.73e-4
C_2H_6	.952	.0995	.0917	.0828
C_3H_6		5.53e-4	5.03e-4	4.46e-4
C_3H_8		.640	.568	.492
C_4H_{10}			.0613	.0515
C_5H_{12}				.0613

Lorentz-Lorenz Theory of the Refractive Index

The Lorentz-Lorenz theory of the refractive index is derived in a number of texts[4]. In the case of spherically or cubically symmetric arrangement of molecules the local electric field E_{loc} is related to the macroscopic electric field E by

$$E_{loc} = E + \frac{4\pi}{3}P \quad . \qquad (1)$$

The $4\pi P/3$ term is the contribution to the local field due to the macroscopic induced polarization P of the surrounding molecules. In the case of a liquid, the spherical symmetry is provided by the randomness of the molecular orientations and positions. Equation 1 is only valid if the molecule is much smaller than the wavelength of light.

The local electric field induces a polarization on the molecule αE_{loc}, and a polarization per unit volume of

$$P = N\alpha E_{loc} \qquad (2)$$

where α is the polarizability of the molecule, and N is the number density. Substituting one equation into another and using

$$(\varepsilon - 1)E = 4\pi P \qquad (3)$$

gives the relation between the dielectric constant ε (and the index of refraction through $n^2=\varepsilon$) and the molecular polarizability

$$N\,\alpha\frac{4\pi}{3} = \frac{\varepsilon - 1}{\varepsilon + 2}. \qquad (4)$$

This is the Lorentz-Lorenz relation. It is useful to define a *molar refractivity* as

$$A = \alpha\frac{4\pi}{3}N_a \qquad (5)$$

where N_a is Avogadro's number. Then we have

$$\frac{\varepsilon - 1}{\varepsilon + 2} = \frac{n^2-1}{n^2+2} = \frac{\rho}{MW}A = \eta A \quad . \qquad (6)$$

Where ρ is the density, MW is the molecular weight, and

$$\eta \equiv \frac{N}{N_a} \qquad (7)$$

is the concentration in moles per unit volume.

Let us refer to the product (ηA) as the *refractivity*. The refractive index of a solution is computed through the combined refractivity of its components.

$$(\eta A)_{solution} = \eta_1 A_1 + \eta_2 A_2 + \ldots \qquad (8).$$

Thus for a given product solution specified by $\eta_1, \eta_2, \eta_3 \ldots$, the refractive index is computed by evaluating the molar refractivities of the individual components, summing their weighted contributions through Eqn. 8, and applying Eqn. 6.

The majority of the remainder of the paper concerns the evaluation of the molar refractivities of the hydrocarbons and carbon particulate species under shock conditions.

Room Pressure Molar Refractivities of Hydrocarbons

Using data on the refractive index, molecular weight and density of hydrocarbon species from the CRC Handbook, we have used Eqn. 6 to calculate the room pressure molar refractivities of species likely to be products of the dissociation of benzene. The results are tabulated in Table 2.

Table 2. Room pressure molar refractivities of hydrocarbons. Computed from CRC Handbook[5] data for sodium D light. Liquids were at 20°C, and gases were assumed to be ideal at standard temperature and pressure.

Species	Formula	MW	density	index	A
Alkanes					
hydrogen	H_2	2.02	STP *gas*	1+1.390e-4	2.076
methane	CH_4	16.04	STP *gas*	1+4.437e-4	6.626
ethane	C_2H_6	30.07	STP *gas*	1+7.558e-4	11.29
propane	C_3H_8	44.11	0.5005	1.2898	15.963
butane	C_4H_{10}	58.13	0.5788	1.3326	20.636
pentane	C_5H_{12}	72.15	0.6262	1.3575	25.270
hexane	C_6H_{14}	86.18	0.6603	1.3751	29.882
heptane	C_7H_{16}	100.21	0.6838	1.3877	34.559
octane	C_8H_{18}	114.23	0.7025	1.3974	39.193
nonane	C_9H_{20}	128.26	0.7176	1.4054	43.846
decane	$C_{10}H_{22}$	142.29	0.7300	1.4102	48.317
Alkenes					
ethene	C_2H_4	28.05			10.7[a]
propene	C_3H_6	42.08			15.5[b]
butene	C_4H_8	56.12	0.5951	1.3465	20.11
benzene	C_6H_6	78.12	0.8787	1.5011	26.198
diamond	C	12.01	3.51	2.4173	2.113[c]
acetylene	C_2H_2	26.04			9.2[d]

[a]Computed from molar refractivity of liquid C_2H_3Cl, accounting for contribution due to chlorine. See page E-223 of ref. [5].
[b]Computed from C_3H_5Cl as above[a].
[c]Equation 6 is valid for crystalline materials of cubic symmetry.
[d]Computed from sum of parts, according to rule on page E-223 of ref. [5].

For the alkanes, where the number of hydrogen atoms to carbon atoms is given by $H=2C+2$, the molar refractivity is accurately described by

$$A=1.038H + 2.558C \qquad (9)$$

implying that each alkane carbon contributes 2.558 and each hydrogen 1.038 toward the molar refractivity of the molecule.

Note that benzene has a greater molar refractivity than that computed through this "alkane rule", and diamond has a lesser value. *This is the fundamental reason the solution's refractive index is predicted to change through the chemical reaction.* On a per atom basis, the refractivity of carbon is highest when it is in a form that has unsaturated bonds such as benzene and lowest in a tightly single–bonded form such as diamond.

Pressure Dependance of the Hydrocarbon Molar Refractivity

We must account for the effect of pressure on the molar refractivities of the hydrocarbons listed in Table 2. By inspecting the measured pressure dependant refractivities of several shocked liquids reported in the literature, and fitting to a common empirical behavior, we can estimate the change in molar refractivities under 15 GPa shock loading.

Figure 1 shows the measured[6,7,8] refractive index of several shocked liquids plotted versus density.

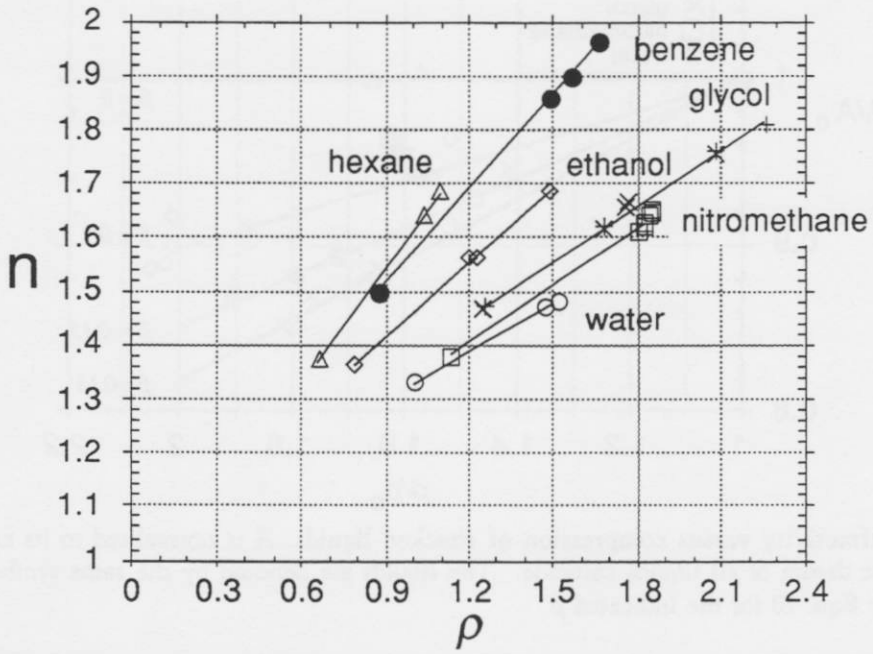

Figure 1. **Refractive Index of Shocked Fluids** versus shock density. Lines are for the eyes. Sources: hexane, water, ethanol[6]; glycerol[6,7]; benzene[7]; nitromethane[8].

Although most of the liquids shown here empirically fit the so-called Gladstone-Dale behavior $(n\text{-}1) \propto \rho$, hexane, the only alkane shown, does not. We have not found refractive index shock data on other alkanes.

In Fig. 2 the data is replotted in terms of molar refractivity normalized to its ambient value and plotted versus compression ρ/ρ_0 . We find that the molar refractivity decreases linearly with compression along lines which can be expressed as

$$\frac{A(\rho)}{A_0} = 1 - \beta\left[\rho/\rho_0 - 1\right]. \qquad (10)$$

The slope of the lines are between $\beta = 0$ and $\beta = 0.18$. Benzene obeys $\beta = 0.15$. Intuitively, we would expect the polarizibility of a molecule to decrease when the molecule contracts as the liquid is compressed. We find this to be the case, except for hexane which remains constant. We have no reason to expect the molar refractivity to increase with compression, and expect that the hydrocarbons of Table 2 will fall somewhere between these two slopes. Therefore, we will take Eqn. 10 with $\beta = 0.1 \pm 0.1$ to describe all the non-benzene liquid hydrocarbons of that Table.

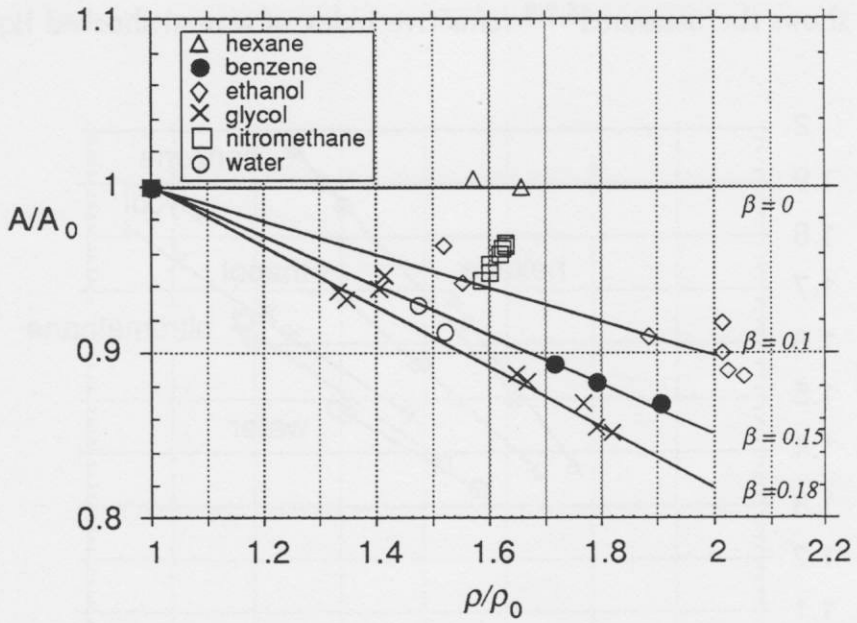

Figure 2. **Molar refractivity versus compression of shocked liquids.** A is normalized to its unshocked value, thus the first datum of all liquids coincide. The liquids are denoted by the same symbols as in Fig. 1. The lines satisfy Eqn. 10 for the indicated β.

According to the shock Hugoniot of benzene[9], at 15 GPa $\rho/\rho_0 = 1.92$. Thus A for benzene is reduced to 86.2% of its ambient value, and for the other hydrocarbons 91±9%. These are tabulated in the first column of Table 3.

Table 3. **Estimated molar refractivities (A) at 15 GPa, and itemized refractivity of endpoint solution.** ($V\eta$) is the number of moles per mole reactant benzene of species in endpoint solution, in a volume V. Only species with significant concentration are listed. The third column is the contributed refractivity (times the volume.)

Species	A(15 GPa)	$V\eta$(moles)	$V(\eta\ A)$
benzene-reactant	22.6	1	22.6
H_2	1.89	0.1420	0.268
CH_4	6.03	0.007280	0.044
C_2H_6	10.27	0.08280	0.850
C_3H_6	16.14	0.0004460	0.007
C_3H_8	14.53	0.4920	7.149
C_4H_{10}	18.78	0.05150	0.967
C_5H_{12}	23.00	0.06130	1.410
Σhydrocarbon product refractivities			10.7±1[a]

[a]Range obtained from recalculating the contributions with $\beta = 0$ and $\beta = 0.20$.

Molar Refractivity for Ellipsoidal Particles with Anisotropic Dielectric Constant

Next we must compute the molar refractivity of carbon when it is in particulate form. To be general we model the particle as an ellipsoid, with semiradii a, b, and c. If the carbon is in the graphite phase it is likely that the particles are platelet-like. We can model such a particle as an oblate spheroid (a=b), a>c with an oblateness ratio a/c. Since

graphite has very anisotropic properties, we allow for a tensor dielectric constant. Fortunately, the principal axes of the dielectric tensor can be taken to coincide with the principle axes of the ellipsoidal shape, for this means that the tensors are diagonal and that the relations governing the optical properties along each principle axis are independent.

The reader is referred to R. Jones[10] for the derivation of the generalized dielectric ellipsoid solution, and to van de Hulst[11] for useful formulae. Only the highlights are reproduced here.

For an ellipsoid in a uniform applied field E_{out} there is a uniform field E_{in} inside

$$\vec{E}_{in} = \vec{E}_{out} - \mathbf{L}\, 4\pi \vec{P} \qquad (11)$$

where P is the polarization inside the ellipsoid, and **L** is a diagonal tensor dependant on the ratios between the principle semiradii. For arbitrary values of the semiradii, **L** is given by an integral expression stated in Reference [10,11]. The sum rule

$$L_{11} + L_{22} + L_{33} = 1 \qquad (12)$$

holds for any shape. Thus, for a sphere $L_{ii}=1/3$. For the special case of an oblate spheroid, a=b, c<a

$$e^2 = \left(\frac{a}{c}\right)^2 - 1, \quad L_{33} = \frac{1+e^2}{e^2}\left(1 - \frac{1}{e}\arctan e\right) \qquad (13)$$

and L_{22} and L_{11} are found with Eqn. 12. As the spheroid becomes more oblate L_{33} approaches 1 and L_{22}, L_{11} approach 0.

The result of the derivation is that for an ellipsoidal particle with a volume V_p, the diagonal elements of the polarizability tensor are given by

$$\alpha_{ii} = \frac{V_p}{4\pi}\frac{(\varepsilon_{ii} - 1)}{[1 + L_{ii}(\varepsilon_{ii} - 1)]} \qquad (14)$$

where ε_{ii} are the diagonal elements of the dielectric constant of the material in bulk form. Multiplying by $4\pi/3$ and Avogadro's number, and dividing by the number of atoms per particle gives us the molar refractivity per particulate atom

$$A_{ii} = \frac{MW}{\rho}\frac{(\varepsilon_{ii} - 1)}{3[1 + L_{ii}(\varepsilon_{ii} - 1)]} \qquad (15)$$

where ρ is the density of the particulate material in bulk form.

Note that for the case of a spherical particle, $L_{ii} = 1/3$ and for an isotropic dielectric constant, as is the case with diamond, that Eqn. 15 is identical with Eqn. 6, the molar refractivity of a liquid or cubically symmetric solid. This means that the molar refractivity of carbon in diamond form is independent of the size of the diamond particle. However, the assumption of a uniform field in the derivation restricts us to particle sizes smaller than the wavelength of light.

Now in a liquid the particle orientation will be random, and the effective value for the molar refractivity obtained by averaging over all angles is rather simple since the tensor is diagonal:

$$A_{eff} = \frac{1}{3}(A_{11} + A_{22} + A_{33}) \qquad (16)$$

We will define the effective value of the molar refractivity as the value that can be used in Eqns. 6 and 8, as if the particles were spherical and isotropic.

Molar Refractivity of Spheroidal Graphitic Particles

ROOM PRESSURE

Because graphite is highly anisotropic we expect particles of this form to be non-spherical and most likely platelet-like. (The report[12] cited above observed graphitic particles in ribbon form, although the aspect ratio between the length and the width of the ribbon was not very large.) For calculational simplicity, we will assume that the graphite is an oblate spheroid with a variable equatorial diameter to thickness ratio (a/c).

To compute the molar refractivity we need the dielectric tensor describing bulk graphite. We have measured the complex dielectric constant of single crystalline graphite (grade ZYA from Union Carbide) at 632.8 nm by ellipsometry of light reflected off its basal plane. Light was reflected at incident angles of 50° and 70° to obtain an average value for the complex dielectric constant

$$\varepsilon_{\|graphite} = 6.5\pm1.5 - i\ 10.5\pm1 \qquad (18)$$

This corresponds to n=3.1±0.15 – i1.7±0.15. Since according to Snell's law the angle of propagation of the light transmitted into the graphite is of the order 15° - 20° from the normal to the basal plane, we take this measurement to be representative of the component of ε parallel to the basal plane. The lack of obvious color of the graphite surface suggests ε does not have a significant wavelength dependance in the visible regime.

It was not possible on our sample to make an ellipsometry measurement of a surface orthogonal to the basal plane, so for the dielectric constant in this direction we must make an educated guess based on the physics of the origin of its polarizability. This is elaborated in Appendix A. Our estimate for room pressure is

$$\varepsilon_{\perp graphite} = 1.6 \qquad (19)$$

The effective value for A, averaging over all angles for a spheroidal particle is

$$A_{eff} = \frac{1}{3}(2A_{\|} + A_{\perp}) \qquad (20)$$

Because $A_{\|}$ is already larger than $A_{\perp}$ and weighted twice as much in Eqn. 20, A_{eff} is not sensitive to estimation errors in $\varepsilon_{\perp}$.

The result for the room pressure value of A_{eff} for graphite spheroids is plotted in Fig. 3 versus oblateness (a/c). The calculation is repeated with $\varepsilon_{\perp}$ twice as large to show that the variation due to mis-estimating $\varepsilon_{\perp}$ is not as significant as the variation due to the particle geometry.

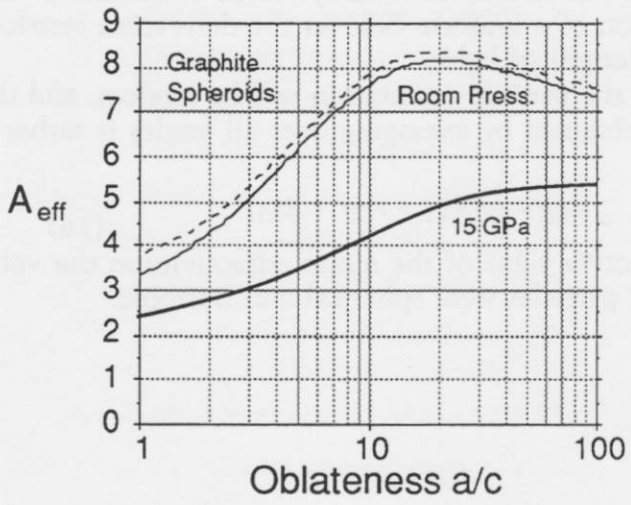

Figure 3. **Effective molar refractivity of spheroidal graphitic particles** versus oblateness. The effective value of A accounts for random particle orientation. To show the insensitivity of the result to $\varepsilon_\perp$, A_{eff} for the room pressure case is recomputed after doubling $\varepsilon_\perp$ and replotted as the dashed curve.

AT 15 GPA

We must estimate the value of $\varepsilon_{||}$ and $\varepsilon_\perp$ appropriate for graphite at 15 GPa, where according to the shock Hugoniot[15], its density has increased by 20%. Fig. 4 shows $\varepsilon_{||\,graphite}$ and $\varepsilon_{diamond}$ in the complex plane. Note that the real part of graphite's dielectric constant (6.5) is similar to that of diamond

$$\varepsilon_{diamond} = n^2 = 5.84 \qquad (21)$$

This suggests that Re(ε) is roughly constant as graphite is compressed.

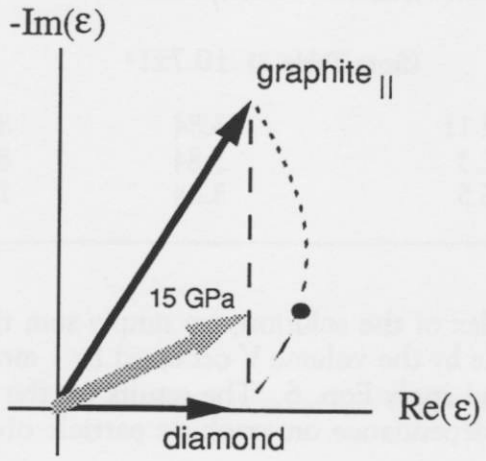

Figure 4. **Dielectric constants of graphite and diamond in the complex plane.** Similarity between the real parts suggests that Re(ε) will be roughly constant through the compression of graphite. A simple model in Appendix B indicates that $\varepsilon_{||\,graphite}$ follows the dashed curve, with a 15 GPa value indicated by the dot.

In Appendix B, a simple model for the dielectric constant of carbon transforming between the graphitic and diamond structures predicts that the locus of $\varepsilon_{||}$ in the complex plane makes a curved path to the right of the vertical, as suggested by the dashed curve in the Figure, and that Im(ε) at 15 GPa is about 1/3 of its initial value. This decrease in Im(ε) is consistent with an observed increase in transmittance of compressed single crystalline graphite measured in a diamond anvil cell by Stishov[16] (See Fig. B3). However, we have no measurements on Re(ε) to similarly corroborate the model's prediction that at 15 GPa Re(e)≥6. Since we prefer to be conservative in our estimate of the refractivity of graphitic particles we will assume that under compression ε follows the vertical line of the Figure; that at 15 GPa Re(ε) is given by its room pressure values and that the imaginary part has decreased by a factor of 3:

$$\varepsilon_{||15GPa} = 6.5 - i\,3.5, \qquad \varepsilon_{\perp 15GPa} = 1.6 \qquad (22)$$

conservative in our estimation for $\varepsilon_{graphite}$, this represents a probable minimum value for A_{eff} for a given oblateness.

Net Refractive Index of Solution

Table 4 summarizes the estimated values of the contributions to the net refractivity from the hydrocarbons and from carbon in its different particulate forms. The values for a graphite spheroid will range between the values given by graphite spheres and graphite platelets (infinitely oblate spheroids).

Table 4. Summary of estimated refractivity contributions at 15 GPa and computation of net refractivity of a benzene product solution. V is volume containing 1 mole of reactant benzene.

Species	A(15 GPa)	$V\eta$(moles)	$V\eta A$
reactant			
benzene	22.6	1	22.6
products			
Σhydrocarbons	(from Table 3)	10.7±1[a]	
carbon particulates			
diamond spheres	2.11	3.84	8.10
graphite spheres	2.3	3.84	8.8
graphite platelets	5.5	3.84	21.1

[a]Range for β=(0,0.2)

To compute the refractive index of the solution, we simply sum the appropriate contributions in Table 4, divide by the volume V occupied by 1 mole of benzene compressed to 15 GPa (V = 46.3 cm^3), and apply Eqn. 6. The results for the refractive index are tabulated in Table 5, and its dependance on graphitic particle oblateness for that case is shown in Fig. 5.

Table 5. Calculated refractive index for 15 GPa benzene product solutions using the Nellis endpoint distribution of Table 1 and different particulate forms. Platelets are spheroids with infinite oblateness.

Solutions	n(15 GPa)
unreacted shocked benzene	1.965
reacted solutions	
with diamond spheres	1.75±.05[a]
with graphite spheres	1.79±.05[a]
with graphite platelets	2.75±.1[a]

[a]Range for β=(0,0.2)

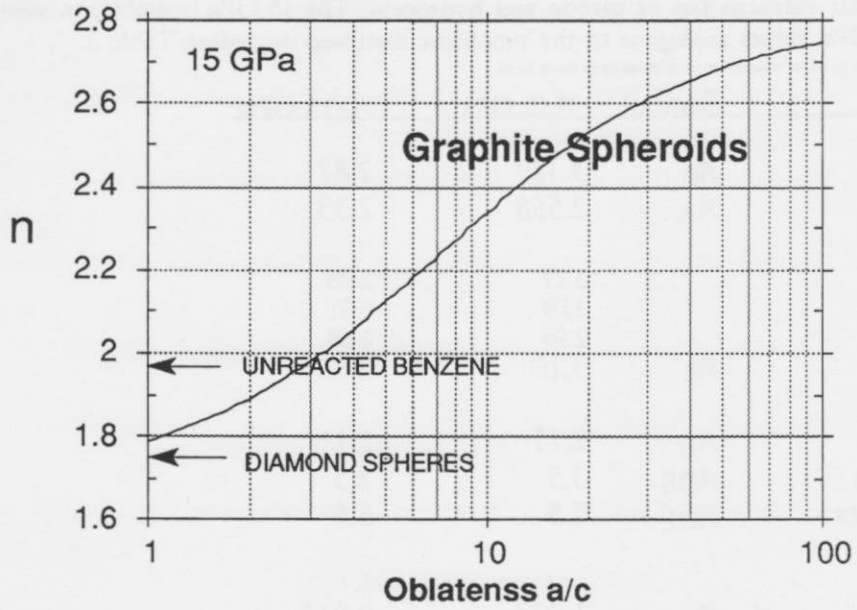

Figure 5. **Calculated final refractive index** of shocked benzene solution for different particulate morphologies. The endpoint distribution of Table 1 was assumed.

Per Atom Refractivities

We have calculated above the refractive index of a shocked solution of benzene dissociation products presuming a distribution of product species. We would now like to generalize our result to arbitrary distribution, so that one can judge the effect of changing the endpoint distribution, and so that in the period before chemical equilibrium is established, one can trace the evolution of n as it travels along an arbitrary reaction path trajectory.

Since the number of carbon and hydrogen atoms is conserved in the dissociation, it is useful to consider the molar refractivities of the hydrocarbons on a *per atom* basis, rather than the per molecule basis in which they are currently expressed. (For particulate carbon, the two quantities are the same.) Let $\mathcal{A}$ denote the per atom molar refractivity. We have already seen through Eqn. 9 that alkanes the per atom contributions can be identified as

$$\mathcal{A}_C = 2.558 \qquad \mathcal{A}_H = 1.038 \qquad (23)$$

for carbon and hydrogen respectively at room pressure. Since we are not constrained, let us assume that $\mathcal{A}_H = 1.038$ in all hydrocarbons and compute the corresponding $\mathcal{A}_C$ by deducting the hydrogen contribution from the values of A given in Table 2. These are tabulated in Table 6 for room and 15 GPa pressure.

Table 6. **Per atom molar refractivities of carbon and hydrogen.** The 15 GPa hydrocarbon values were estimated from the 0 GPa values analogous to the procedure discussed preceding Table 2.

Species	Symbol	$\mathcal{A}$ (0 GPa)	$\mathcal{A}$ (15 GPa)
Carbon, in			
benzene	$\mathcal{A}_B$	3.329	2.87
alkanes	$\mathcal{A}_A$	2.558	2.33
alkenes			
ethene		3.27	2.98
propene		3.09	2.81
butene		2.95	2.68
average	$\mathcal{A}_E$	3.10	2.82
diamond	$\mathcal{A}_D$	2.11	2.11
graphite spheres	$\mathcal{A}_{GS}$	3.5	2.3
graphite platelets	$\mathcal{A}_{GP}$	7.5	5.5
Hydrogen, in			
alkanes	$\mathcal{A}_{HA}$	1.038	0.945
benzene	$\mathcal{A}_{HB}$	1.038	0.895[a]

[a] $\mathcal{A}_{HA}$ differs from $\mathcal{A}_{HB}$ at 15 GPa because we assumed different pressure dependencies for the host species.

Arbitrary Reaction Trajectory

If one has J different carbon containing species involved in the dissociation of benzene, then an equation expressing the conservation of carbon will involve the sum of J terms equalling a constant, with each term representing the amount of carbon in the form of a particular species. Since each of these terms is non-negative, the trajectory of the dissociation reaction (following the carbon) can be mapped onto a J-1 dimensional hyper-tetrahedron. Since in the higher dimensions it is difficult to visualize the hyper-tetrahedrons and realize them on a sheet of paper, it is desirable to make simplifications so that the reaction trajectory can be represented by 3 or 4 terms on a triangle or tetrahedron respectively.

First, the results of the equilibrium calculation tabulated in Table 1 indicate that alkane hydrocarbons are stable, alkenes are unstable, and alkynes and benzene are very unstable. Thus we will ignore alkynes as having an insignificantly small concentration. Benzene is similarly unstable, but its concentration is obviously finite at t=0; the amount of carbon in the form of benzene will be the first reaction coordinate. Secondly, we will consider only one form of carbon particulate at one time. Thirdly, because $\mathcal{A}_C$ and $\mathcal{A}_H$ have been shown to be nearly identical for all the alkanes of Table 2, we can represent the distribution of alkanes by a single mean alkane species. (Hydrogen is an alkane species). The amount of carbon in alkane form will be the third reaction coordinate. Fourthly, all the alkenes will be similarly represented by a mean alkene species. According to Table 6, $\mathcal{A}_C$ for the three alkenes listed range within 6% of the average value, so this is a reasonable simplification. We will then have 4 reaction coordinates.

Our discussion below is for 1 mole of reactant benzene. The simplified reaction is

$$C_6H_6 \Rightarrow m'_B\, C_6H_6 + m'_P\, C + m'_A\, C_\alpha H_{2\alpha+2} + m'_E\, C_\gamma H_{2\gamma} \quad (24)$$

where m'_B, m'_P, m'_A and m'_E denote the number of molecules (in moles) of benzene, particulate carbon, mean alkane and mean alkene respectively. The mean alkane is an

average over the distribution of alkanes and has a mean carbon number α,

$$\alpha = \left[\sum_i i\, m'_{Ai}\right]\left[\sum_i m'_{Ai}\right]^{-1} \qquad m'_A = \sum_i m'_{Ai} \tag{25}$$

where m'_{Ai} are the amounts of individual alkanes of size i. The expression for the mean alkene is analogous.

From Eqn. 24 we obtain the conservation equations for carbon and hydrogen:

$$6 = m_B + m_P + m_A + m_E \tag{26}$$ and

$$6 = m_B + \frac{2\alpha + 2}{\alpha} m_A + 2 m_E \tag{27}$$

where

$$m_B \equiv 6\, m'_B, \quad m_P \equiv m'_P, \quad m_A \equiv \alpha\, m'_A, \text{ and } m_E \equiv \gamma m'_E \tag{28}$$

The unprimed m are the number of moles of carbon in the form of a particular species.

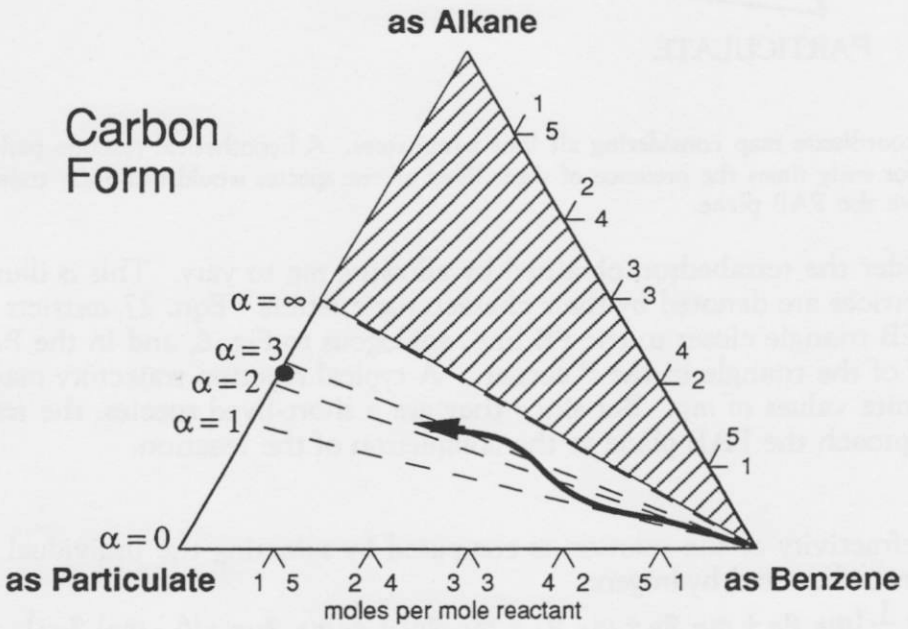

Figure 6. **Reaction coordinate map** following the form of carbon, for 1 mole reactant benzene. The vertices correspond to carbon being completely in the associated species. The coordinate for benzene for example is normal to, and zero at the Alkane-Particulate line. α is the mean alkane size. Lines of constant α are drawn as dashes. The region above the $\alpha=\infty$ line is unattainable. The endpoint distribution of Table 1 is indicated by the dot. A hypothetical reaction trajectory is shown as curved path.

Consider first the plane described by Eqn. 26 when m_E=0. Since all m must be non-negative, the boundaries of the plane form an isosceles triangle when viewed normal to the plane. This is illustrated in Fig. 6. At each vertex, the 6 moles of carbon is completely in the form of the given species. Eqn. 27 further constrains the solution to the half of the triangle adjacent to the Particulate-Benzene edge. The endpoint distribution of Table 1 is represented by a dot on the Particulate-Alkane line. A hypothetical reaction trajectory would begin at the Benzene vertex and would essentially end on the Particulate-Alkane line in the vicinity of the dot. (The residual amount of benzene at the end of the dissociation is insignificant.) The exact endpoint position will of course depend on the character of the shock.

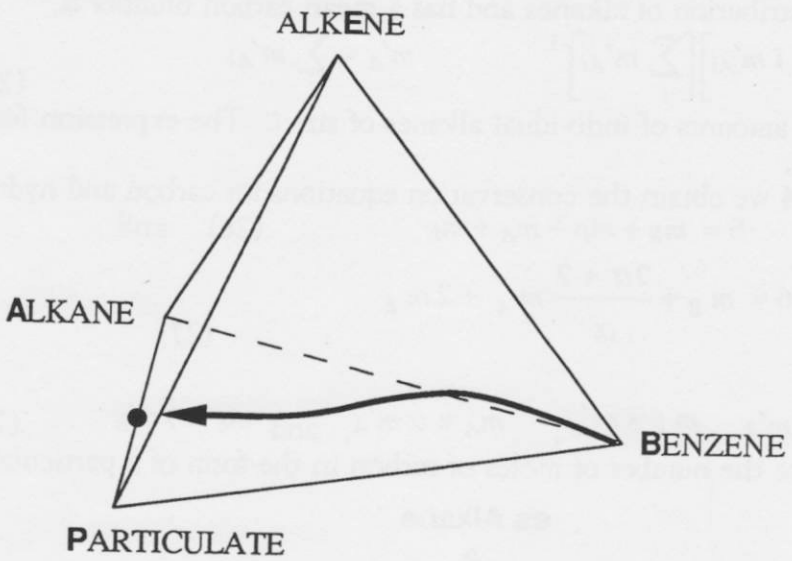

Figure 7. **Reaction coordinate map considering all four parameters.** A hypothetical reaction path is shown demonstrating how for early times the presence of short lived alkene species would cause the trajectory to temporarily rise above the PAB plane.

Now consider the tetrahedron obtained by allowing m_E to vary. This is illustrated in Fig. 7. The vertices are denoted by their characteristic letters. Eqn. 27 restricts us to the half of the PEB triangle closer to the PB line, analogous to Fig. 6, and in the PAE plane, to the half of the triangle in the P corner. A typical reaction trajectory may initially rise to finite values of m_E. But since they are a short-lived species, the trajectory will inevitably approach the PAB plane at the completion of the reaction.

Final Result

The net refractivity of the solution is computed by summing the individual contributions from carbon and hydrogen:

$$(\eta A)_{solution} = \frac{1}{V}\{m_B\,\mathcal{A}_B + m_P\,\mathcal{A}_P + m_A\,\mathcal{A}_A + m_E\,\mathcal{A}_E\} + \frac{1}{V}\{m_B\,\mathcal{A}_{HB} + (6 - m_B)\,\mathcal{A}_{HA}\} \quad (29)$$

Note that the hydrogen contribution from the both the alkenes and alkanes are represented by the very last term. For the case where the particulates are graphite platelets, we use $\mathcal{A}_{GP}$ for $\mathcal{A}_P$ and calculate the refractive index from Eqn. 29 and Eqn. 6. This is plotted as contours on the PAB and PEB planes in Fig. 8.

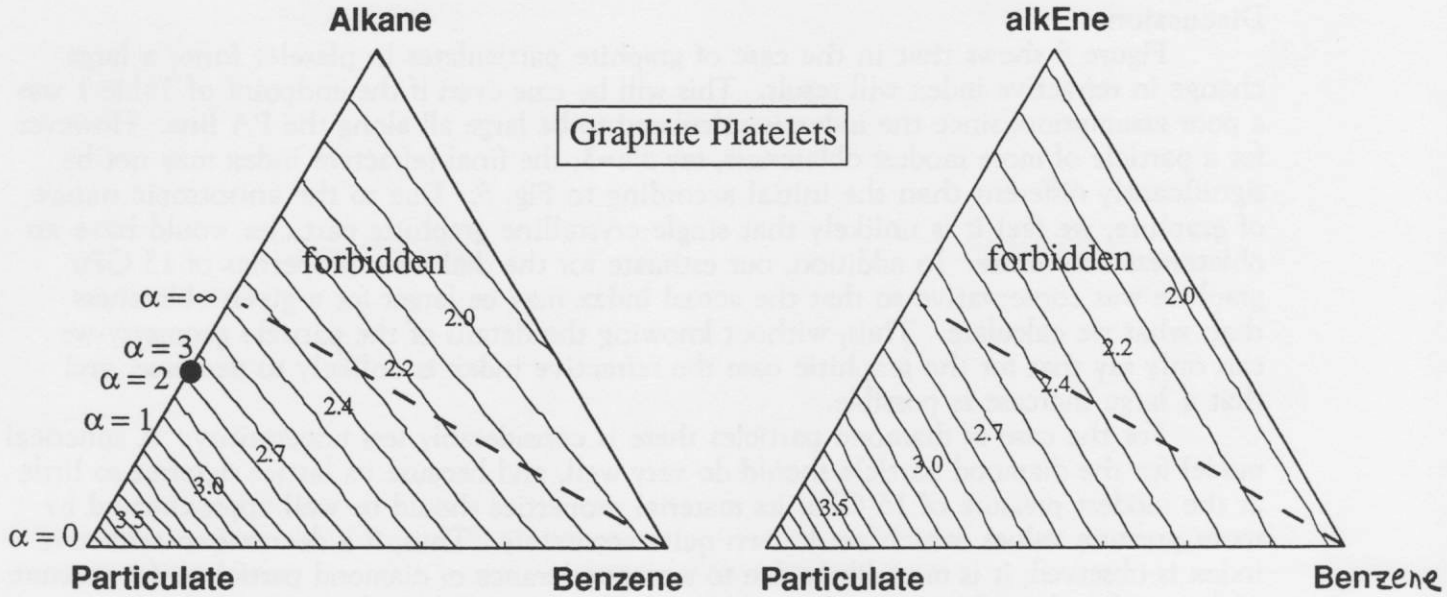

Figure 8. Contour map of calculated refractive index of 15 GPa shocked benzene in the graphitic platelet case, on the PAB and PEB planes. The dot indicates the endpoint of Table 1.

Figure 9 shows the result for diamond particles in the PAB and PEB planes.

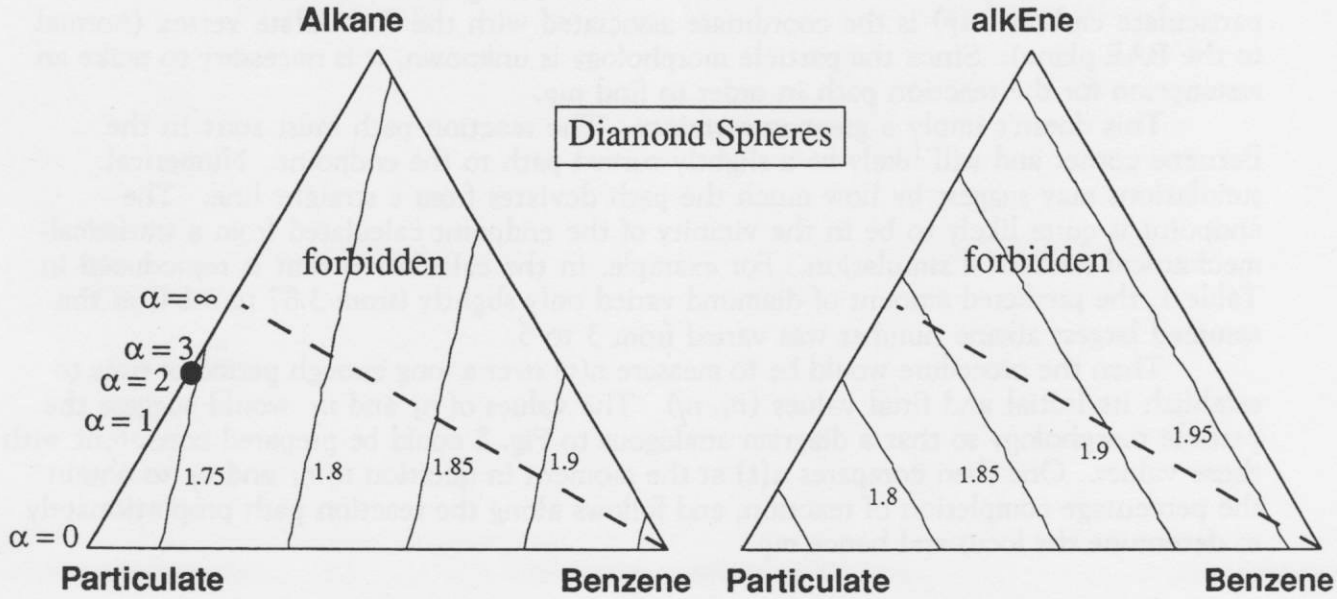

Figure 9. Same as Fig. 8, but for the case when the particulates are diamond spheres.

Discussion

Figure 8 shows that in the case of graphite particulates in platelet form, a large change in refractive index will result. This will be true even if the endpoint of Table 1 was a poor assumption, since the index is calculated to be large all along the PA line. However, for a particle of more modest oblateness, say a/c=3, the final refractive index may not be significantly different than the initial according to Fig. 5. Due to the anisotropic nature of graphite, we feel it is unlikely that single crystalline graphitic particles would have an oblateness near unity. In addition, our estimate for the dielectric properties of 15 GPa graphite was conservative so that the actual index may be larger for a given oblateness than what we calculate. Thus, without knowing the details of the particle geometry we can only say that for the graphitic case the refractive index is unlikely to decrease, and that a large increase is possible.

For the case of diamond particles there is considerably less uncertainty. A spherical model for the diamond particle should do very well, and because its lattice deforms so little at the modest pressure of 15 GPa, its material properties should be well approximated by room pressure values, which are known quite accurately. Thus, if a decrease in refractive index is observed, it is most likely due to a preponderance of diamond particles. (A mixture of diamond and graphitic particles would probable not produce a decreasing index.)

A question which has not yet been addressed is how well are the material properties of the particles modeled by bulk values. Considering the short time scale of their formation, how ordered are the crystals, and how "dirty" are the particles because of inclusion of hydrocarbons?.

Particulate Carbon Amount

As mentioned in the introduction, one of the motivations for measuring the refractive index is to provide a value for the instantaneous amount of particulate carbon, so that the particle size can be extracted from Mie scattering data. The amount of particulate carbon (m_P) is the coordinate associated with the Particulate vertex (normal to the BAE plane). Since the particle morphology is unknown, it is necessary to make an assumption for the reaction path in order to find m_P.

This doesn't imply a great uncertainty. The reaction path must start in the Benzene corner and will likely be a slightly curved path to the endpoint. Numerical simulations may suggest by how much the path deviates from a straight line. The endpoint is quite likely to be in the vicinity of the endpoint calculated from a statistical-mechanical numerical simulation. For example, in the calculation that is reproduced in Table 1, the predicted amount of diamond varied only slightly (from 3.87 to 3.84) as the assumed largest alkane number was varied from 3 to 5.

Then the procedure would be to measure $n(t)$ over a long enough period of time to establish its initial and final values (n_i, n_f). The values of n_i and n_f would suggest the particle morphology so that a diagram analogous to Fig. 8 could be prepared consistent with those values. One then compares $n(t)$ at the moment in question to n_i and n_f to obtain the percentage completion of reaction, and follows along the reaction path proportionately to determine the locus and hence m_P.

Appendix A

Estimation of room pressure $\varepsilon_{\perp \text{graphite}}$

To investigate the origin of the dielectric properties of graphite we need to generalize the relationship derived earlier between the dielectric constant and the molar refractivity to include a lattice of arbitrary symmetry. The internal molar refractivity so derived will characterize the polarizability of the carbon atom within the graphitic lattice.

We will denote it by B to distinguish it from the external molar refractivity A discussed previously that characterizes the polarizability of the particle as a whole (even though its value is expressed on a per atom basis.) Then by comparison with $B_{diamond}$ and of $B_{||graphite}$, $B_{\perp}$ can be estimated, from which $\varepsilon_{\perp}$ is calculated.

The dielectric properties of a lattice of arbitrary symmetry is discussed by Mueller[16] and by Kittel[17]. We start by generalizing Eqn. 1. The local electric field will be related to the applied field by

$$\vec{E}_{loc} = \vec{E} + \mathbf{K}\, 4\pi \vec{P} \qquad \text{(A1)}$$

where **K** is a diagonal tensor expressing the lattice symmetry and is analogous to the geometry factor **L** introduced in Eqn. 11 for the generalized ellipsoid solution. **K** follows the sum rule $\Sigma K_{ii}=1$, so that for a cubic or spherical symmetry $K_{ii}=1/3$ and Eqn. A1 is identical to Eqn. 1.

By a derivation analogous to Eqns. 1 through 6, we obtain

$$B_{ii} = \frac{MW}{\rho} \frac{(\varepsilon_{ii} - 1)}{3[1 + K_{ii}(\varepsilon_{ii} - 1)]} \qquad \text{(A2)}$$

Note that for a cubic lattice, this equation is identical to Eqn. 6. Thus for diamond B is equivalent to A.

For non-cubic lattices $K \neq 1/3$. Mueller computes K for tetragonal[16] and simple hexagonal[18] lattices versus aspect ratio c/a. $K_{||}$ and $K_{\perp}$ denote the components parallel and normal to the basal plane respectively, and $2K_{||}+K_{\perp}=1$. These are plotted in Figure A1. For large c/a, $K_{||}$ asymptotically approaches the lines $K_{||}=0.370(c/a)$ and $K_{||}=0.359(c/a)$ for simple hexagonal and tetragonal lattices respectively.

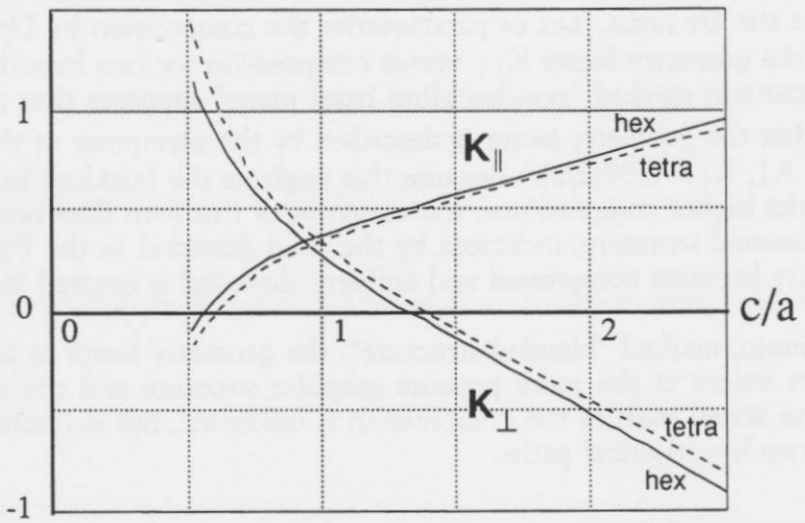

Fig. A1. **Geometry factors for simple hexagonal[16] and tetragonal[18] lattices** versus aspect ratio c/a of unit cell. $2K_{||}+K_{\perp}=1$. For large c/a, $K_{||}$ approaches the lines 0.370(c/a) and 0.359(c/a) for simple hexagonal and tetragonal lattices respectively.

The graphite lattice is obtained from the simple hexagonal lattice by translating every other basal plane by a/2. For large c/a, the effect of the translation of the planes on K should be slight, so we will model the ambient graphite lattice as a simple hexagonal lattice with c/a=2.36 [ref 19]. Thus $K_{||}=0.873$ and $K_{\perp}=-0.746$. Then from our measured values of $\varepsilon_{diamond}$ and $\varepsilon_{||graphite}$, (Eqns. 17,18) and Eqn. A2 we calculate

$$B_{||graphite} = 1.94 - i\,0.159 \qquad \text{(A3)}$$

and we already know that

$$B_{\perp diamond} = A_{\perp diamond} = 2.11. \qquad (A4)$$

Note the similarity of the real parts. We expect that the polarizability of graphite parallel to the basal planes is due to a combination of bound and free electrons, and that for diamond is due to bound electrons only. Thus we associate the bound contribution with the real part having a magnitude near 2. Since graphite conducts very poorly normal to the basal plane, we expect the polarizability in that direction to be due only to bound charges,and therefore estimate

$$B_{\perp graphite} = 2.0. \qquad (A5)$$

Using Eqn. A2 with the same K values we work backwards to obtain

$$\varepsilon_{\perp graphite} = 1.6. \qquad (A6)$$

Appendix B

Estimation of 15 GPa $\varepsilon_{||\,graphite}$

As graphite is compressed there are two quantities that are changing: the crystal structure, and the internal molar refractivity B. In principle, knowledge of both allows calculation of ε, but in practice the evaluation of K for an arbitrary structure can be tedious. The calculation below is done making simplifying assumptions on the behavior of K and B for several different scenarios that are likely to encompass the actual behavior.

Under shock compression of 15 GPa, graphite increases its density by 20%[9]. A pseudopotential calculation of the transformation of graphite to diamond[19] suggests that in this range of compression the change in intra-layer bond length and buckling angle is not significant, so that the compression is accommodated mostly by the change in inter-layer spacing, and hence the c/a ratio. Let us parameterize the compression by $1/\rho$. Figure B1 plots the change in the geometry factor $K_{||}$ versus compression for two hypothetical transformations. The scenario marked "non-buckling basal plane" supposes that c/a varies linearly with $1/\rho$, and that the geometry factor is described by the asymptote of the simple hexagonal curve of Fig. A1, $K_{||}=0.37(c/a)$. Because this neglects the buckling in the basal planes which occurs at the higher compressions, the endpoint of this path does not coincide with the locus of the diamond structure, indicated by the solid diamond in the Figure. (The difference in density between compressed and ambient diamond is ignored in this analysis.)

In the other scenario, marked "blended structure", the geometry factor is assumed to vary linearly between its values at the room pressure graphite structure and the diamond structure endpoints. The actual path of the compression is unknown, but is likely to fall in the range between the two hypothetical paths.

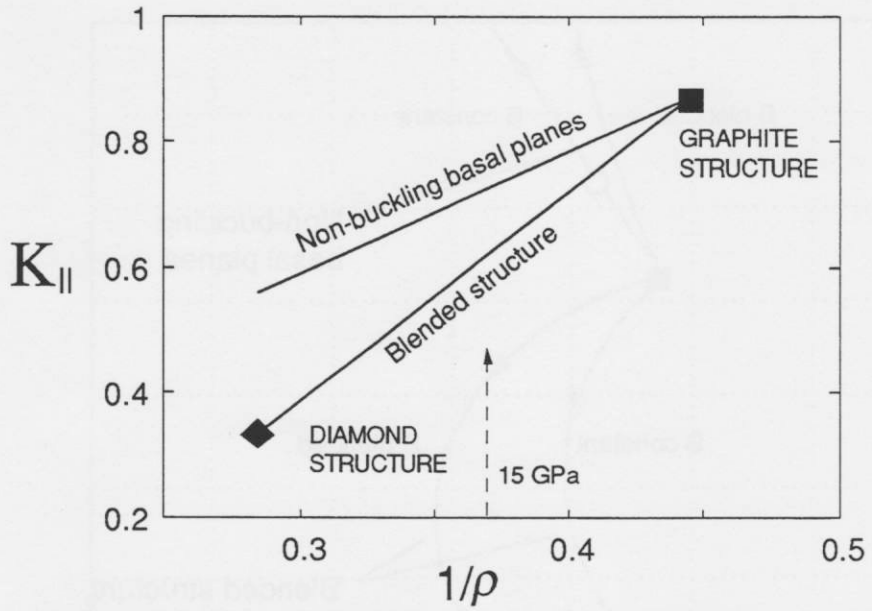

Figure B1. **Geometry factor versus 1/density** for two hypothetical structural transformations. The line marked "non-buckling basal planes" assumes K is given by the asymptote of the curve for simple hexagonal structure of Fig. A1, taking $c/a \propto 1/\rho$. The second transformation assumes K varies linearly between the room pressure graphite and diamond endpoints, represented by the square and diamond respectively. The 20% increase in the density of graphite at 15 GPa is indicated.

Similarly for B, we consider a scenario where B is smoothly blended between its graphitic and diamond values (given by Eqns. A3 and A4), and a scenario where B is held constant at the graphitic value. Since $\mathrm{Re}(B_{||})$ is nearly identical in the two cases, this distinction essentially affects only $\mathrm{Im}(B_{||})$.

For the four scenario combinations, $\varepsilon_{||}$ is calculated through the inverse of Eqn. A2:

$$\varepsilon = 1 + \left[\frac{MW}{3\rho B} - K\right]^{-1} \qquad \text{(B1)}$$

and plotted in the complex plane in Fig. B2. The result shows that the non-buckling basal plane assumption leads to divergent behavior in $\varepsilon_{||}$. In this case the path of $\varepsilon_{||}$ is sensitive to choice of B and moves away from the diamond locus with compression. We feel this is unlikely to be physical since we expect $\mathrm{Im}(\varepsilon_{||})$ to decrease with compression and eventually approach the diamond locus. This misbehavior suggests that either the assumption of non-buckling is poor, or that the geometry factor K for compressed graphite structure is not well approximated by the simple hexagonal value at higher compressions.

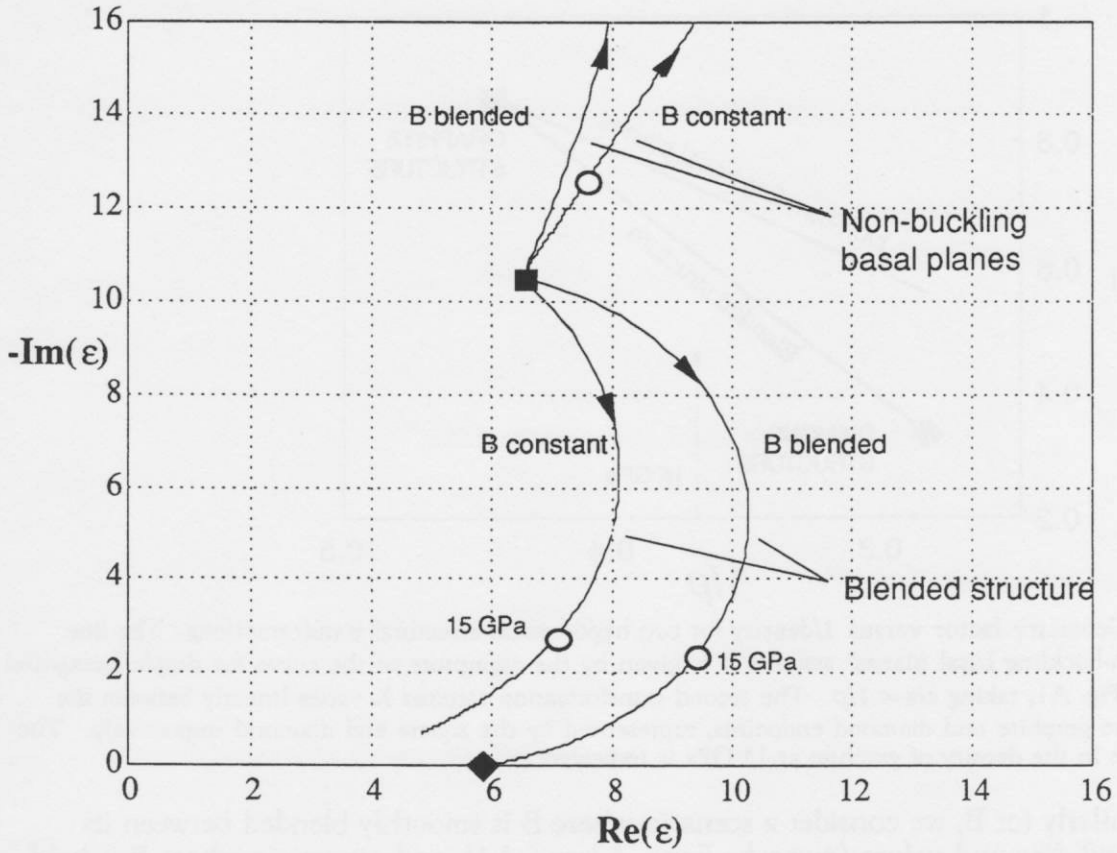

Figure B2. **Calculated paths of $\varepsilon_{||}$ in the complex plane during compression** for the four scenario combinations described in the text. The loci for ambient graphite and diamond are marked by the square and diamond respectively. The open circles mark the 15 GPa values (20% compression). In the case of B blended/non-buckling basal planes, the path curves rapidly up and counter-clockwise; the 15 GPa point is off the chart at $\varepsilon=7-i\,31$.

In contrast, the case of the blended structure is well-behaved: the path is relatively insensitive to B and it moves toward the diamond locus. It is interesting to note that it is not necessary to have a decreasing Im(B) to produce a decreasing Im(ε), as demonstrated by the B constant/ blended structure case.

The behavior for the blended structure case is consistent with observations of the optical absorption length of single-crystalline graphite normal to the basal plane in a diamond anvil cell by Stishov[15]. His results are plotted in Fig. B3 in terms of Im(n) versus pressure. They show that Im(n) decreases by a factor of 60 at 42 GPa. (Since Im(ε)=2 Re(n) Im(n) and Re(n) is not expected to change more than 30% over this range, we can take Im(ε) $\propto$ Im(n).) An interpolative curve drawn between the room pressure datum and the higher pressure data suggests a drop by a factor of 2-10 in Im(n) at 15 GPa. This is consistent with the calculation in the blended structure case, where the 15 GPa points are marked with open circles and show a decrease in Im($\varepsilon_{||}$) of about a factor of 3. In contrast, the calculated paths for the non-buckling case are not consistent with the measured decrease of Im(n) at 42 GPa.

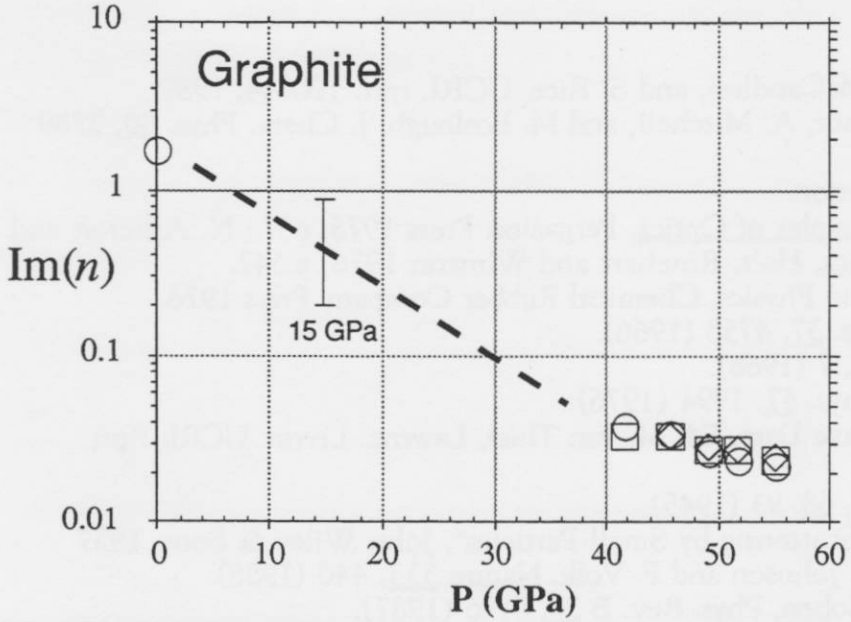

Figure B3. **Measured imaginary part of refractive index versus pressure** for single crystalline graphite for photon energies 2 eV (circles), 2.5 eV (squares), and 3 eV (diamonds). The high pressure data was from absorption length data measured by Stishov[15] in a diamond anvil cell for light propagating normal to the basal plane. The room pressure value was measured by ellipsometry. A simple interpolation suggest the 15 GPa value would range a factor of 2 to 10 times lower than the room pressure value.

In conclusion, we believe the actual path of $\varepsilon_{||}$ to be similar to the blended structure case because of its consistency with Stishov's measurements. Because of the uncertainty of the actual path, and because we have no measurement of $\mathrm{Re}(\varepsilon_{||})$ for comparison, it is difficult to predict $\mathrm{Re}(\varepsilon_{||})$ at 15 GPa more specific than $\mathrm{Re}(\varepsilon_{||}) \geq 6$. However, because we have a physical measurement of $\mathrm{Im}(\varepsilon_{||})$, and because our calculated result for $\mathrm{Im}(\varepsilon_{||})$ appears to be relatively insensitive to assumptions on B, we are more confident in predicting that $\mathrm{Im}(\varepsilon_{||})$ at 15 GPa will be about 1/3 its ambient value.

Estimation of 15 GPa $\varepsilon_{\perp graphite}$

When we perform an analogous calculation for $\varepsilon_{\perp}$, we find it is much less sensitive to choice of path. We consider the case where $B_{\perp}$ is constant at 2.0, and where it varies linearly between 2.0 and the diamond value of 2.11, and we consider both paths of $K_{||}$ plotted in Fig. B1 and use $K_{\perp}=1-2K_{||}$. We find that for both scenarios of $B_{\perp}$, $\varepsilon_{\perp}$(15 GPa)=1.8 for the non-buckling plane cases, and $\varepsilon_{\perp}$(15 GPa)=2.0 for the blended structure cases.

Acknowledgements

Thanks to Neil Holmes for his support and many enthusiastic discussions. This work was performed under the auspices of the U.S. Department of Energy (LLNL) under contract No. W-7405-Eng-48.

References

[1] N. Holmes, G. Otani, P. McCandless, and S. Rice, UCRL rprt. 100644, 1989.
[2] W. Nellis, F. Ree, R. Trainor, A. Mitchell, and M. Boslough, J. Chem. Phys. 80, 2789 (1984).
[3] F. Ree, private communication.
[4] M. Born and E. Wolf, Principles of Optics, Pergamon Press 1975, p87.; N. Ashcroft and N. Mermin, Solid State Physics, Holt, Rinehart and Winston 1976, p.542.
[5] Handbook of Chemistry and Physics, Chemical Rubber Company Press 1976.
[6] T. Ahrens, Jrnl. Appl. Phys. 37, 4758 (1966).
[7] K. B. Yushko, JETP Lett. 7, 7 (1968).
[8] D. Hardesty, Jrnl. Appl. Phys. 47, 1994 (1976).
[9] Compendium of Shock Wave Data, Ed. M. van Thiel, Lawrnc. Livrm. UCRL Rprt. #50108, 1977
[10] R.Clark Jones, Phys. Rev., 68, 93 (1945).
[11] H. van de Hulst, "Light Scattering by Small Particles", John Wiley & Sons, 1957
[12] N. Greiner, D. Phillips, J. Johnson and F. Volk, Nature 333, 440 (1988).
[13] K.J. Chang and Marvin Cohen, Phys. Rev. B 35, 8196 (1987).
[14] J.L. Wise and L. C. Chhabildas, Shock Waves in Condensed Matter, Ed. Y. M. Gupta, Plenum Press 1985.
[15] Stishov. unpublished report 1989.
[16] H. Mueller, Phys. Rev. 47, 947 (1935).
[17] C. Kittel, "Introduction to Solid State Physics", John Wiley, 3rd Ed..
[18] H. Mueller, Phys. Rev. 50, 547 (1936).
[19] S. Fahy, S. Louie and M.L. cohen, Physical Rev B 34, 1191 (1986).